EEET ECOLOGICAL ENGINEERING & ENVIRONMENTAL TECHNOLOGY

Ecological Engineering & Environmental Technology 2024, 25(2), 54–69
https://doi.org/10.12912/27197050/175786
ISSN 2719–7050, License CC-BY 4.0

Received: 2023.11.19
Accepted: 2023.12.15
Published: 2024.01.01

Highlighting Volcanic Outcrops by Mapping Geological Lineaments Using Satellite Data in he Saka Region, North-East Morocco

Abdallah Elaaraj[1,2*], Ali Lhachmi[1], Hassan Tabyaoui[1], Abdennabi Alitane[3,4], Yassine El Yousfi[5]

[1] Sidi Mohamed Ben Abdellah University, Polydisciplinary Faculty of Taza, Natural Resources and Environment Laboratory, Department of Geology, 1223, Fez, Morocco

[2] Sidi Mohamed Ben Abdellah University, Faculty of Science and Technology, Engineering Sciences and Techniques Center, Environment Department, 1223, Fez, Morocco

[3] Moulay Ismail University, Faculty of Sciences, Geoengineering and Environment Laboratory, Research Group "Water Sciences and Environment Engineering", Department of Geology, 50050, Meknes, Morocco

[4] Vrije Universiteit Brussels (VUB), Hydrology and Hydraulic Engineering Department, 1050, Brussels, Belgium

[5] Abdelmalek Essaadi University, National School of Applied Sciences Al Hoceima, Water and Environment Management, Laboratory of Applied Sciences (LSA), 93030, Tétouan, Morocco

* Corresponding author's e-mail: abdallah.elaaraj.ac.ma

ABSTRACT

The Saka region and its environs are situated in the northeastern part of Morocco. This study aimed to optimize automated lineament extraction based on the comparing of Landsat-8 optical satellite data with Sentinel-2B for enhanced analysis. The research delved into the structural lineaments within the Saka region, with the objective of advancing the understanding of lineament extraction techniques. Remote sensing techniques were employed to extract and map these lineaments Furthermore, the study sought to elucidate the distribution and genesis of volcanism in the Saka region and its surroundings in the context of geodynamics. The availability of optical and multispectral remote sensing datasets, including those from Landsat-8 OLI and Sentinel-2B, characterized by medium and high spatial resolutions, enhances the efficiency and simplicity of lineament mapping – an essential component of any structural geological investigation. However, due to the differences in spatial resolution and sensitivity to land cover, the outcomes from these diverse data sources were derived with varying resolutions display variability. The spatial resolution of the images significantly influences the precision and clarity of the retrieved lineaments. The findings underscore a strong correlation between lineament directions (primarily NE-SW, E-W, NW-SE) and faults, i.e., correspond to the distribution of volcanic outcrops in the Saka area and its vicinity. For validation purposes, the lineaments extracted through directional filtering were compared to the manually obtained lineaments, alongside lineaments digitized from the pre-existing neotectonic map (faults) as well as satellite images depicting lineaments in the study area. Density analysis was employed to investigate the correlation between the concentration of lineaments and the distribution of pre-existing faults. Additionally, the geological map was utilized to refine the correlation between density distribution and the spatial orientations of volcanic rock formations in the study area.

Keywords: Landsat-8Oli, Sentinel-2B, automatic lineament extraction, mapping lineaments, Saka, volcanic rocks.

INTRODUCTION

A crucial component of any structural geological inquiry has always been the representation of linear structural segments on the map, often known as „lineaments," on the surface of the Earth. Lineaments show the structure of the foundational rocks, formed through various tectonic processes (deformational) events throughout the geological history of a region (Ramli et

al., 2010). The prospection, exploration, and mining of different mineral deposits are all based on structural geological investigations and lithological mapping, which are collectively referred to as geological mapping. Comprehending the origin and deposition of comparable mineral resources necessitates structural studies of the geological units surrounding the mineral deposits. Identification of significant structural events and their timing in ore districts enables the construction of models explaining the genesis of ore formation. Furthermore, comprehending the structural geology of a region is essential for understanding its geological history, which is necessary for simulating numerous ancient paleoclimatic and paleogeographic events (Negredo et al., 2007). Consequently, automatic, quicker methods for geological mapping of such areas must be developed, using satellite imagery, computational software, and algorithms that would aid and direct field investigations. As their spatial and spectral characteristics change as they extend, linear objects in remote sensing data can be difficult to identify (Wang, 1993). For diverse applications, including the identification of road networks, extracting linear features from digital satellite data (Singh and Garg, 2013; Valero et al., 2010), stream networks (Martinez et al., 2009; Paiva et al., 2015), and geological lineaments (Hashim et al., 2013; Maged and Mazlan, 2010) is essential; thus, several algorithms have been developed. Faults, dykes, shear zones, and folds are examples of geological lineaments, which are expressions of the underlying geological structure. Because of their relationship to hydrothermal mineralization, linear to curvilinear faults, dykes, and shear zones are especially fascinating for aiding mineral exploration (Manuel et al., 2017; Pour and Hashim, 2014). However, these features are equally useful for hydrogeological (Bhuiyan, 2015; Takorabt et al., 2018) and tectonic research (Arian and Nouri, 2015; Masoud and Koike, 2017). Identifying key structural units, analyzing structural deformation patterns, locating geological boundaries, and discovering mineral deposits can all be done using faults, dykes, and shear zones (Glasser and Ghiglione, 2009; Pour and Hashim, 2014). In the absence of a sedimentary or regolithic cover, mineral deposits frequently form clusters along specific locations along deep crustal structures (Hein et al., 2013; Lund et al., 2011). Economic factors make it crucial to comprehend the structural mechanisms underlying hydrothermal ore deposits over deep crustal discontinuities, but this is still up for debate. Some scientists contend that fault bends are the main factor influencing ore clusters, while others think fault intersections are crucial (Lu et al., 2016). However, both situations can play a role in the genesis of hydrothermal ore deposits. Regardless of the methods, finding geological lineaments can assist and connect the surface lineament expressions to underlying structural discontinuities, which eventually supports mapping mineral prospectivity. Since remote sensing has made such significant strides, it is now possible to characterize lineaments by utilizing a wide range of sources and techniques. As a consequence, automated methods are becoming more popular than manual ones, which are challenging, time-consuming, and heavily dependent on the accuracy of the analysis (Masoud and Koike, 2006).

The study sought to investigate and understand structural lineaments in the Saka region using remote sensing techniques, primarily to extract and map these lineaments. Additionally, it aimed to use this lineament data to gain insights into the distribution and implementation of volcanism in the area, which is significant for understanding the region's geodynamics. The availability of optical and multispectral remote sensing data, such as Sentinel-2B andLandsat-8 Oli, is harnessed to improve the accuracy and simplicity of lineament mapping, a crucial aspect of structural geological research. The study acknowledged the impact of spatial resolution on the precision and clarity of the extracted lineaments.

The subsequent sections of this article were organized as follows: Section 2 delves into the Geographic and Geological setting. Section 3 outlines the materials and methods employed in this study. Finally, Section 4 provides the discussion and conclusion of the paper.

STUDY AREA

Geographic setting

The study area, encompassing Saka and its surroundings, is situated in the northeastern part of Morocco (Fig. 1) and spans an area of 7779 km².

It extends across longitudes ranging from 3.95°W to 2.84°W and latitudes from 34.26°N

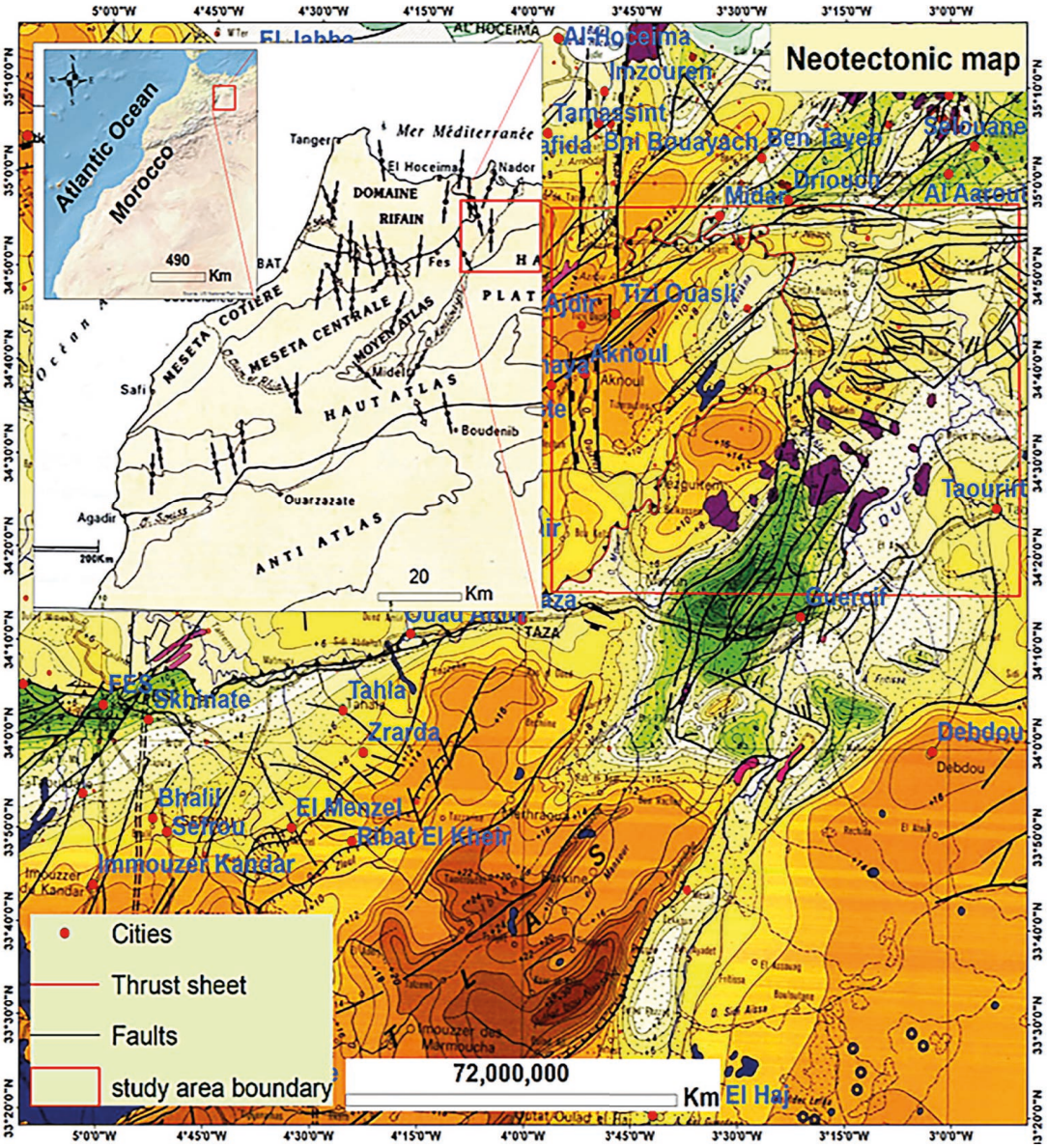

Figure 1. Geographical location of the study area

to 34.95°N. The study area spans two structural domains, namely the Meso-Atlasic and the Rifian (as depicted in Figure 1). The region experiences an average annual rainfall of 225 mm, indicating a predominantly semi-arid climate (El Kati et al., 2018).

Geological context

The Saka area and its environs, situated in the northeastern part of Morocco between the Rif and the Middle Atlas, are part of the Guercif basin, characterized as a depression filled with Tertiary and Quaternary deposits. This region comprises Triassic and Jurassic sediments forming the substratum, overlain unconformably by Neogene and Quaternary deposits (EL Kati, 2017). Its geological history is notably complex due to its proximity to the Moulouya belt shear zone and the arcuate Rifian front (Bernini et al., 1999). The digitized geological map indicates that the upper Jurassic facies predominantly geologic formation in the study area (24.88%), followed by middle and ancient Quaternary limestone (15.03%), and upper Cretaceous flysch (10.43%).

DATA AND METHODS

On the basis of the literature survey conducted in 1975, it was found that there is no

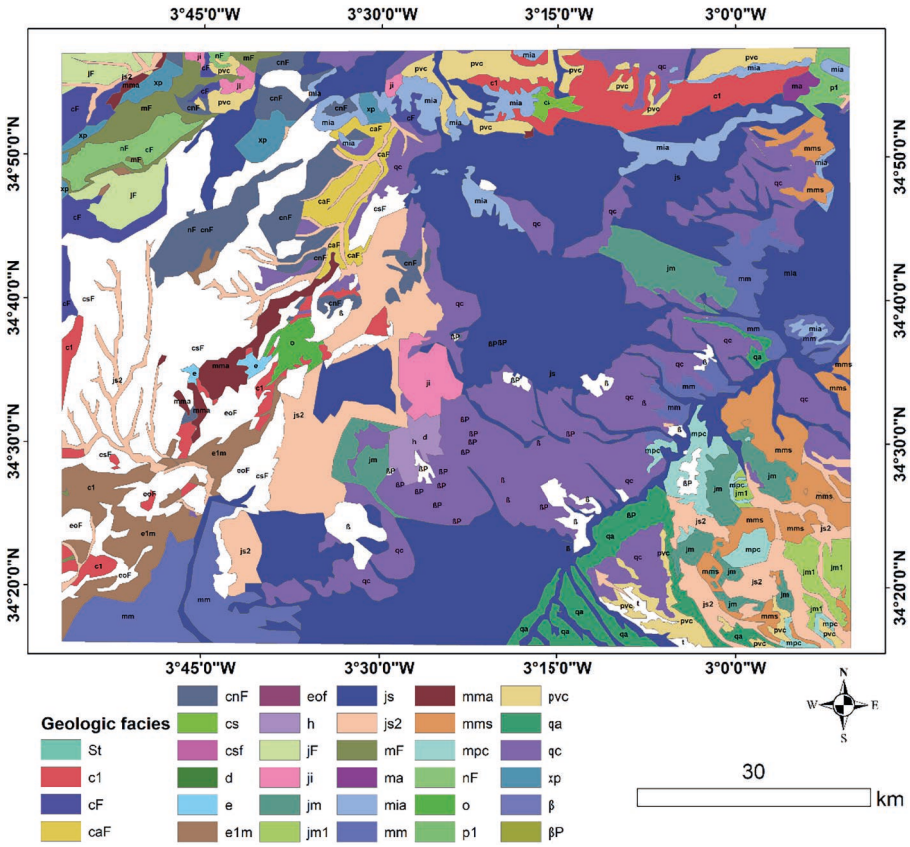

Figure 2. Geological facies, faults, and digitized lineaments in the Saka region and its surroundings. t: Generally intrusive Triassic : gypseous and saliferous, c1: Lower Cretaceous marine, cF: Cretaceous Flysch, caF: Ante-orogenic Cretaceous with Flysch, cnF: Cretaceous and Eocene marly flysch, cs: Upper Cretaceous, csF: Upper Cretaceous to Flysch, d: Devonian, e: Eocene, e1m: White marl with flint, eof: Nummulitic Flysch with Oligocene dominance, h: shale, jF: Flysch, ji: Lias, jm: Middle Jurassic, jm1: Bathonian and Bajocian, js: Upper Jurassic, js2: Insituarian, mF: Miocene Flysch, ma: Ante-orogenic Miocene, mia: Lower Miocene anteorogenic with marly to transgressive facies, mm: Middle Miocene with blue marl facies, mma: Middle Miocene ante-orogenic with blue marl facies with transgressive facies, mms: Middle Miocene with sandy Sahelian facies, mpc: Mio-Pliocene continental, nF: Nummulitic Flysch, o: Marine Oligocene, p1: Marine Pliocene, pvc: Pliocene Villafranchian to conglomerate, qa: Early Quaternary: terraces, qc: Middle and ancient Quaternary limestone, xp: primary or Precambrian (shales or quartzites), β: basalt, βP: Pliocene basalt

single method for detecting geological lineaments in remote sensing. However, the commonly three methods that are used to extract geological lineaments (Ahmadi and Pekkan, 2021): (i) Manual Extraction, (ii) Semi-Automated Extraction, and (iii) Automated Extraction. In this work, only automated and manual lineaments extraction were used.

The lineaments mapping was elaborated using two satellite dataset (Sentinel 2B, Landsat-8 Oli). On the basis of satellite bands, many processing, and techniques were used to determine and filter the lineament's directions in the study area, such as atmospheric, and radiometric for satellite images to provide them with the preliminary focus and prepare them for further analysis. Statistical analysis especially PCA has been used to assess the correlation between the band imagery. This process can be easily applied in the toolbox of ENVI software. The methodology framework defined based on the research questions and hypothesis, is presented in Figure 3. This work was performed using ENVI 5.3, PC GEOMATICA 2016, ArcGIS 10.8, and Rockworks16 software.

Preprocessing

The radiometric correction involves converting digital values into physical units to analyze reflectance. The data from satellite sensors are indeed influenced by various factors which are different in the captor's manufacture, scattering atmospheric absorption, electrical noise, and the

Table 1. Sentinel-2 MSI and Landsat-8 OLI spectral band ranges

Data	Spectral range	Wave length range (μm)	Spatial resolution	Sources
Landsat-8 Oli	1 – Coasta Aerosol 2 – Blue 3 – Green 4 – Red 5 – Near Infrared (NIR) 6 – Short Wave Infrared (SWIR) 1 7 – Short Wave Infrared (SWIR) 2 8 – Panchromatic 9 – Cirrus 10 – Thermal Infrared (TIRS) 1 11 – Thermal Infrared (TIRS) 2	0.433 – 0.453 0.450 – 0.515 0.525 – 0.600 0.630 – 0.680 0.845 – 0885 1.560 – 1.660 2.100 – 2.300 0.500 – 0.680 1.360 – 1.390 10.6 – 11.2 11.5 – 12.5	30 30 30 30 30 30 30 15 30 100 100	(Pinto et al., 2018)
Sentinel 2B image	1 – Coasta Aerosol 2 – Blue 3 – Green 4 – Red 5 – Vegetation Red Edge 6 – Vegetation Red Edge 7 – Vegetation Red Edge 8 – NIR 8a – Vegetation Red 9 – Water vapor 10 – SWIR/Cirrus 11 – SWIR 1 12 – SWIR 2	0.423 – 0.463 0.425 – 0.555 0.525 – 0.595 0.635 – 0.695 0.690 – 0.720 0.725 – 0.755 0.763 – 0.803 0.727 – 0.957 0.845 – 0.885 0.925 – 0.965 1.345 – 1.405 1.520 – 1.700 2.010 – 2.370	60 10 10 10 20 20 20 10 20 60 60 20 20	(Pinto et al., 2018)
Neo-tectonic map	-	-	1:1000 000	
Geologic map			1:500 000	

differences in gaining and linear response of each detector (Begeman et al., 2022).

The atmospheric correction this correction is necessary for the preprocessing of satellite images and is based on use the algorithm of Fast Line-of-sight Atmospheric Analysis of Spectral Hypercube (FLAASH) to isolate the intrinsic surface characteristics from atmospheric effects in the observations (Cooley et al., 2002).

Processing

The principal component analysis (PCA) is a method of data analysis widely used in geological studies (Zhang et al., 2007). It has the advantage of converting correlated variables into new variables that are mutually uncorrelated (Elaaraj et al., 2022). It allows the researcher to reduce the numbers of variables and make the information less redundant.

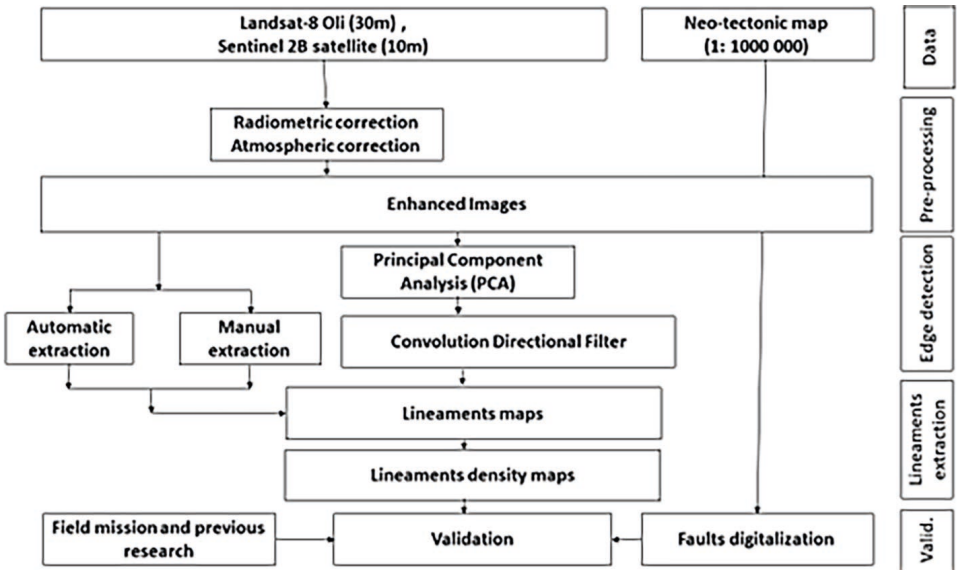

Figure 3. Methodological flowchart of the study

The Lineament extraction can be done in two ways such as manual and automatic (Nguimbous-Kouoh et al., 2019). The current research is centered on the automated extraction of lineaments through satellite imagery, and neotectonic map. During the first step the image filtering was done using the 7×7 directional filters (enhance certain features of the image) for detection of contours and lines, in the second stage, the lineaments are digitally captured from both the satellite images and the neotectonic map of Morocco at scale 1:1 000000 (Table 1).

Verification and validation

The relevance of the methodology is assessed through crucial steps of controlling and validating the directions of extracted lineaments from satellite images. This involves comparing these directions with those of faults digitized from the neotectonic map and examining the distribution of volcanic rock outcrops as indicated in the geological map.

RESULTS AND DISCUSSIONS

Principal component analysis

Principal Component Analysis (PCA) was conducted utilizing specific bands (2, 3, 4, and 8) for Sentinel-2B and bands 1 through 7 for Landsat-8 OLI to determine which bands carry the most valuable information. The resulting PCA images exhibit enhanced spectral contrast, facilitating the successful identification of existing features (Figure 4). PCA is particularly well-suited for lithological mapping, as each lithological unit is distinctly visible in the PCA images. In certain cases, lineaments or faults can be employed to delineate the boundaries between adjacent lithologies. This enables analysts to quickly digitize these boundaries from the PCA images. PCA is often used as a supplementary technique in geological mapping, for example, Suzen et al. (Suzen and Toprak, 1998) utilized PCA as a multi-band analysis to augment the results obtained from directional filters for geological lineaments. The outcomes of this process are presented in Table 2. For the both satellite images used, the novel components generated by this method can account for as much as 95.50% and 95.79% of the original or initial dataset, respectively.

Extraction of lineaments

The lineaments were extracted using both manual techniques (digitization of lineaments) and automatic techniques (directional filters), based on a range of data, through Geomatica 2016 software.

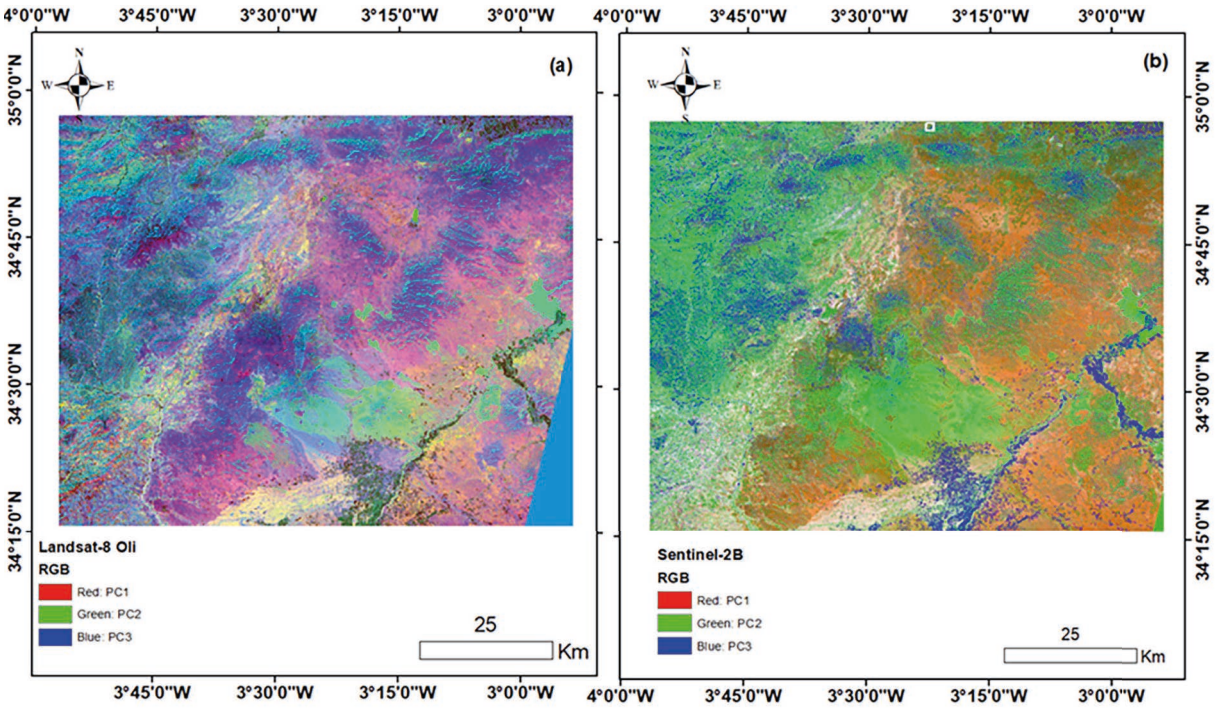

Figure 4. False color composite of PCA 3 (Red), PCA2 (Green), and PCA1 (blue): a)Landsat-8 Oli, b): Sentinel-2B

Table 2. PCA for Landsat-8 Oli and Sentinel-2B

Captor	Component	% Variance	Eigenvalue
Landsat-8Oli	CP1	95.50	0.036733
	CP2	2.52	0.000969
	CP3	1.49	0.000573
	CP4	0.32	0.000124
	CP5	0.09	0.000035
	CP6	0.07	0.000026
	CP7	0.01	0.000003
	Sum	100	0.038463
Sentinel-2B	CP1	95.79	0.015899
	CP2	3.19	0.00053
	CP3	0.93	0.000155
	CP4	0.08	0.000014
	Sum	100	0.016598

Automatic lineaments extraction

The automated extraction of lineaments is performed using computer-aided software, involving several processing steps such as enhancement, filtering, edge recognition, and lineament extraction. Scientists have developed various algorithms to automatically extract lineaments, including the Hough Transform (Wang and Howarth, 1990), Lineament Extraction and Stripe Statistical Analysis (LESSA) (Zlatopolsky, 1992), Segment Tracing Algorithm (STA) (Koike et al., 1995), Canny Algorithm (Maged and Mazlan, 2010), the ADALGEO (Soto-Pinto et al., 2013), TecLines (Rahnama and Gloaguen, 2014), and Lineament Detection and Analysis (LINDA) (Masoud and Koike, 2017). The final lineament map produced by these algorithms is provided in vector format and can be operated by software. Automatic lineament extraction techniques consider such factors as noise, threshold, size, and orientation of linear features (Joshi, 1989). While these automatic methods expedite the analyst's work, they still have limitations. Occasionally, the extracted linear features or lineaments may not precisely correspond to the underlying geological structures. In such cases, the analyst or user needs to evaluate the extracted lineaments or include manual interpretations. Numerous notable studies have applied automated algorithms for the detection of geological faults and lineaments using various types of remote sensing data, including Landsat MSS (Caumon et al., 2009; Tyan and Wang, 1993), Landsat ETM+ (El-Sawy et al., 2016; Mavrantza and Argialas, 2003), ASTER (Soto-Pinto et al., 2013), DEM (Abdullah et al., 2013; Rajendran and Nasir, 2019), multispectral data (Adiri et al., 2017; Masoud and Koike, 2011), and high spatial resolution data like KIONOS (Koçal, 2004)Top of Form

Directional filters (N00, N45, N90 and N135)

Figures 5 and 6 showcase maps of lineaments and corresponding rose diagrams derived from the application of the automated lineament extraction

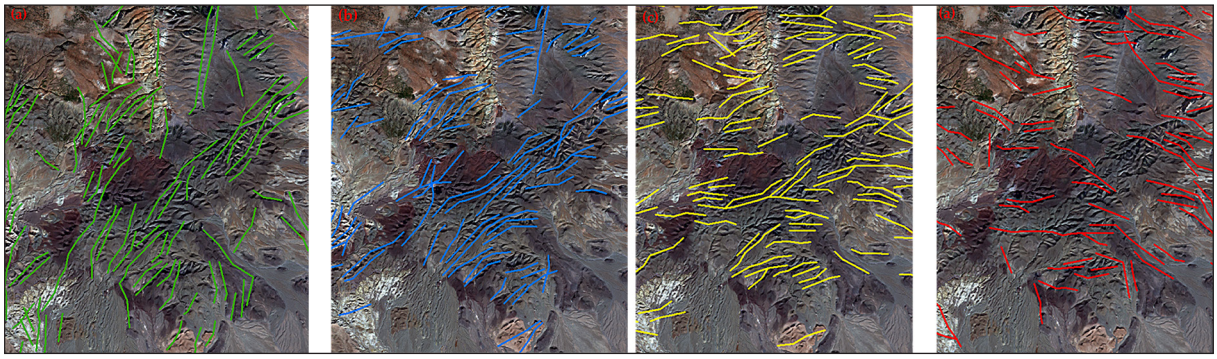

Figure 5. Lineaments auto-extraction using directional filters: N00(a), N45 (b), N90(c), N135 (d)

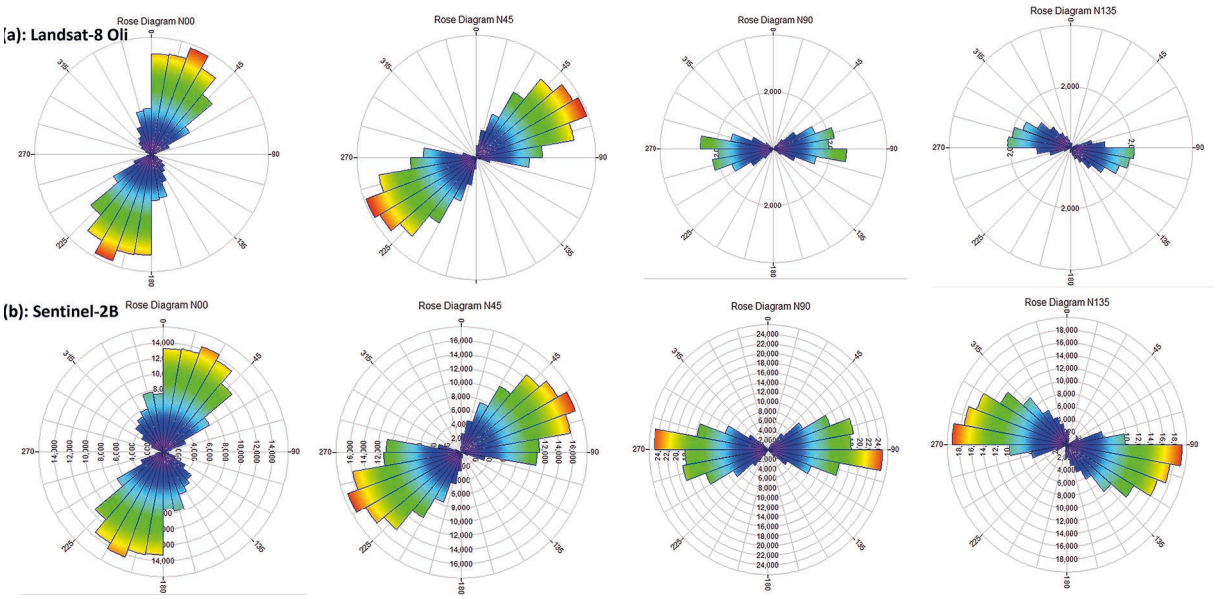

Figure 6. Rose diagrams depict lineaments extracted from lineaments (a) Landsat and (b) Sentineldata using directional filters: N00, N45, N90, and N135 applied to the PCA

method to Landsat 8 OLI and Sentinel 2B satellite images. The directions indicated by both satellite data are consistent. However, the difference between the two datasets lies in the number of the generated lineaments, with Sentinel 2B yielding a greater quantity. The prevalence of lineaments, under the directional filters N00, N45, N90, and N135, varies within the ranges of 0 to 45, 30 to 90, 60 to 110, and 90 to 135, respectively.

Directional filters overlay

The lineament maps and their corresponding rose diagrams, derived from overlaying the outcomes of various directional filters applied in the automatic process of extraction lineament from satellite images (Figure 7), reveal three predominant lineament orientations, listed in order of significance as E-W, NE-SW, and NW-SE. These findings are further supported by the field photographs depicted in Figure 8.

Manual lineaments extraction

The process of manual lineament extraction, particularly well-suited for spatial assessment, encompasses radiometric calibration, atmospheric correction, visual interpretation, and manual lineament delineation. When the primary objective is to identify geological features, manual lineament extraction is employed (Das et al., 2018). The outcomes of manual lineament extraction are contingent on the expertise and specific area of interest of the analyst. Initial efforts in interpreting lineaments included utilizing stereoptic

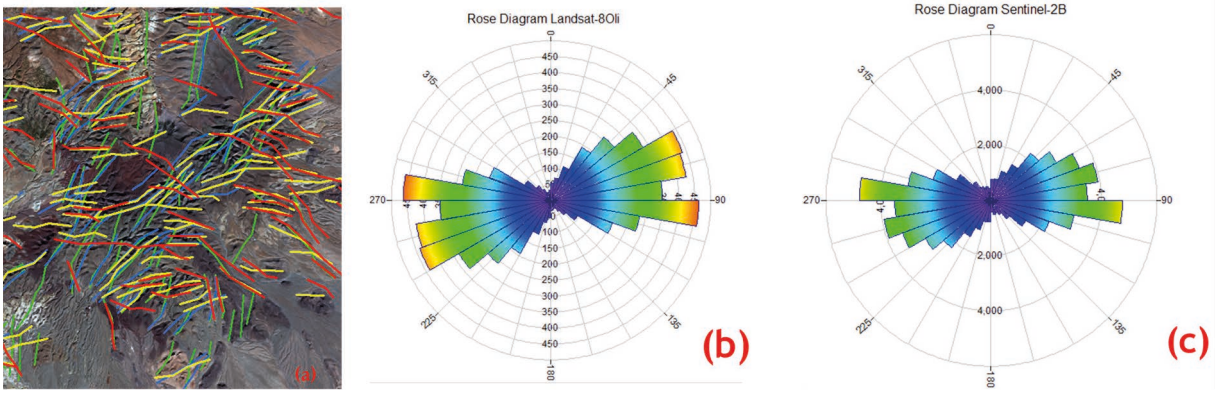

Figure 7. Directional filters overlay (a) and rose diagrams of lineaments extracted from Landsat-8 OLI (b) and Sentinel-2B (c)

Figure 8. The three primary directions of field-observed lineaments, which are E-W, NE-SW, and NW-SE

aerial photographs. In this process, lineaments were marked on transparent overlays and then transferred onto maps (Burns and Brown, 1978; Huntington and Raiche, 1978; Ramli et al., 2010). Many researchers choose high-resolution satellite imagery or digital terrain models (DTM) for the manual extraction of lineaments (Chaabouni et al., 2012; Das et al., 2018). With satellite data, lineaments frequently appear as straight lines or clear edges, identifiable through tonal variations in surface materials (El-Sawy et al., 2016). Accurately classifying lineaments and linking fragmented segments into longer formations heavily relies on the field expertise of the user (El-Sawy et al., 2016; Sarp, 2005). Additionally, image quality is considered a significant factor for enhancing lineament identification in a manual approach (Alshayef et al., 2017). It is worth noting that the manual digitization process is slow, labor-intensive, and subject to subjectivity (Moore and Hastings, 1986).

In Figure 9, a comparison is presented between the results obtained from manual digitization of the neotectonic map (a), satellite images (b, c). For t lineaments (faults) digitized from the neotectonic map, three main lineament directions have been identified, prioritized in the order of significance as E-W, NE-SW, and NW-SE. Conversely, when examining the digitization of Landsat-8 OLI and Sentinel-2B satellite images, the hierarchy of importance in classification shifts to NE-SW,

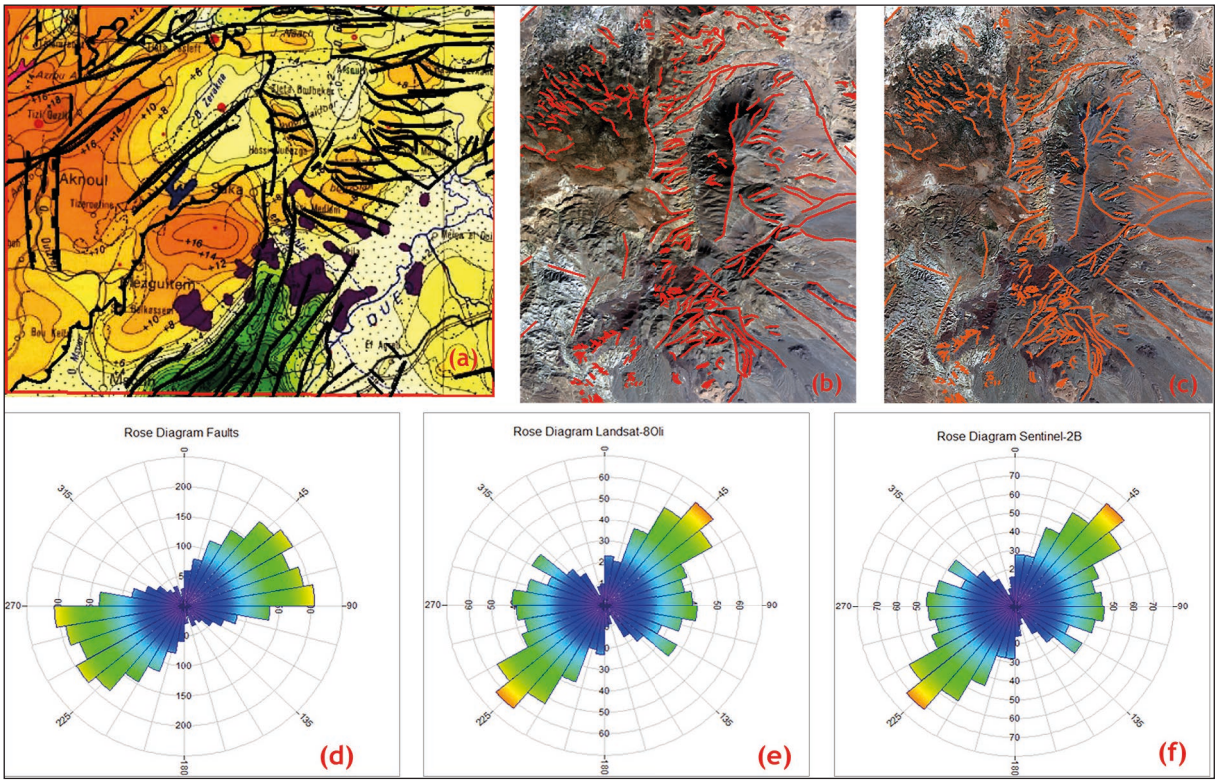

Figure 9. The orientations of lineaments digitized from the Neotectonic map (a), Landsat-8 OLI image (b), and Sentinel-2B image (c), along with their corresponding diagrammatic roses (d, e, and f)

E-W, and NW-SE. This shift is attributed to the high spatial resolution of the satellite images used, particularly Sentinel-2B which boasts a resolution of 10 meters.

Lineament density

The analysis of lineament density is widely recognized as one of the most effective statistical methods for exploring the spatial distribution characteristics of lineaments. It provides valuable insights into the morphological aspects of the land surface (Corgne et al., 2010). Density holds a pivotal role in lineament studies (Corgne et al., 2010; Hashim et al., 2013; Hung et al., 2005; Lachaine, 1999), by furnishing data regarding the number of lineaments in in a specific location (Lachaine, 1999). In this study, density was utilized to examine the connection between the distribution of pre-existing faults and the concentration of lineaments within the investigated area.

Lineament density for directional filters N00

Lineament density in the Saka area and its surroundings differs between Landsat-8 Oli and Sentinel-2B images, ranging from 0 to 10,200 km/km² and 0 to 208,000 km/km², respectively (as shown in Figure 9). The higher frequency of lineaments in the Sentinel data compared to the Landsat data can be attributed to its superior spatial resolution.

Lineament density for directional filters N45

Examining the lineament density map generated from Landsat-8Oli and Sentinel-2B images following the application the N45 directional filter (Figure 10) indicates the presence of extensive fracturing in the study area. The lineament density spans from 0 to 10,500 km/km² in Landsat-8Oli and 0 to 273,000 km/km² in Sentinel-2B images. Occurrences of low and medium densities are relatively infrequent, mainly found and predominate in the central and southwestern regions of the area. In contrast, high and very high densities are concentrated in the northern areas, covering smaller portions of the territory.

Lineaments density for directional filters N90

Contrasting the lineament density maps generated from Landsat-8Oli and Sentinel-2B for the directional filter N90 reveals that the Sentinel-2B data shows higher lineament density in the area compared to Landsat-8Oli. The frequency of Lineaments in the Landsat image ranges from 0 to 11,300 km/km², whereas in the Sentinel image, it varies from 0 to 338,600 km/km².

Lineament density for directional filters N135

In recent years, remote sensing has proven to be a valuable tool in various geological disciplines, especially in the fields of structural geology, tectonics, lithological mapping, and seismic

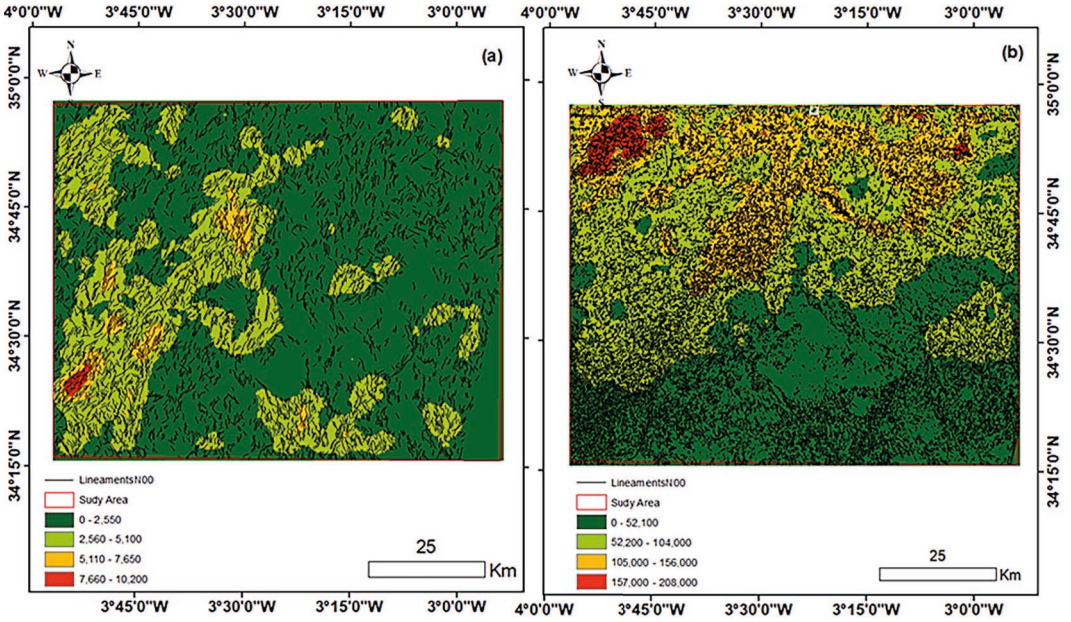

Figure 10. The lineament density for the directional filters N00 extracted from Landsat-8 OLI (a) and Sentinel-2B (b)

monitoring. Within the realm of geology, the term ‚lineaments' collectively encompasses geological features such as faults, fractures, joints, and lithological boundaries. Various remote sensing data sources and analysis methods are available for detecting and studying these geological structures. Consequently, the identification of geological lineaments plays a crucial role in the exploration of mineral deposits linked to hydrothermal activity changes and magmatic processes. Additionally, lineaments are instrumental in assessing natural hazards such as earthquakes and seismic activity, as well as determining groundwater potential and landslide risks. Traditional methods for studying geological lineaments have been costly and time-intensive. Moreover, the physical and geographical characteristics of the research area pose challenges to the use of conventional approaches. Instead, remote sensing technology has emerged as a more efficient means to map geological lineaments, allowing for the identification of faults and their tectonic implications.

The application of preprocessing and processing techniques to Landsat and Sentinel images has proven to be instrumental in generating improved

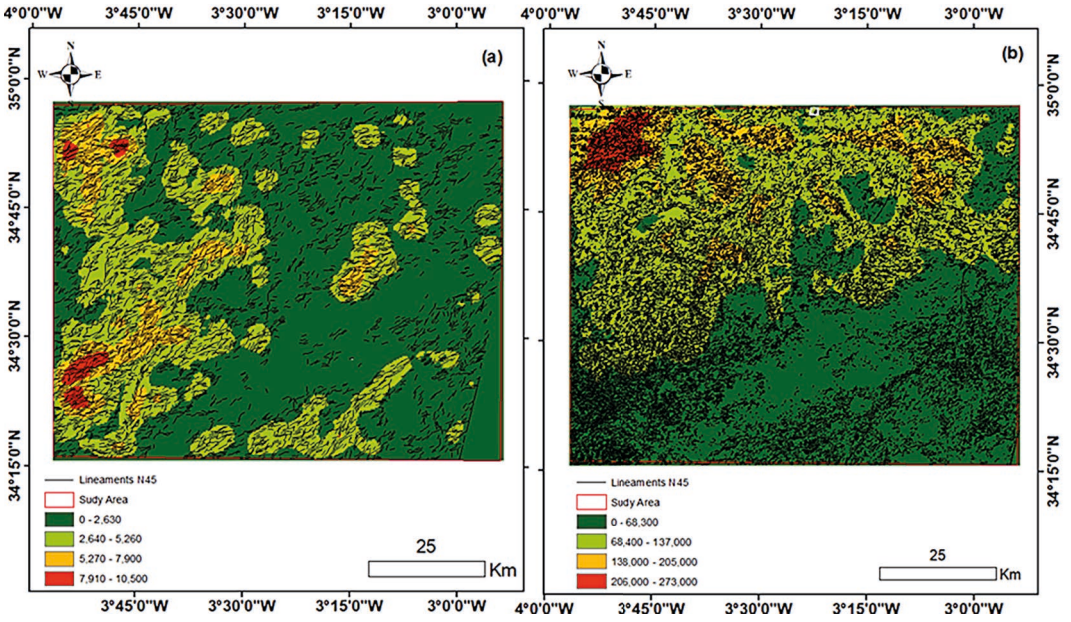

Figure 11. Lineament density corresponding to the N45 directional filters

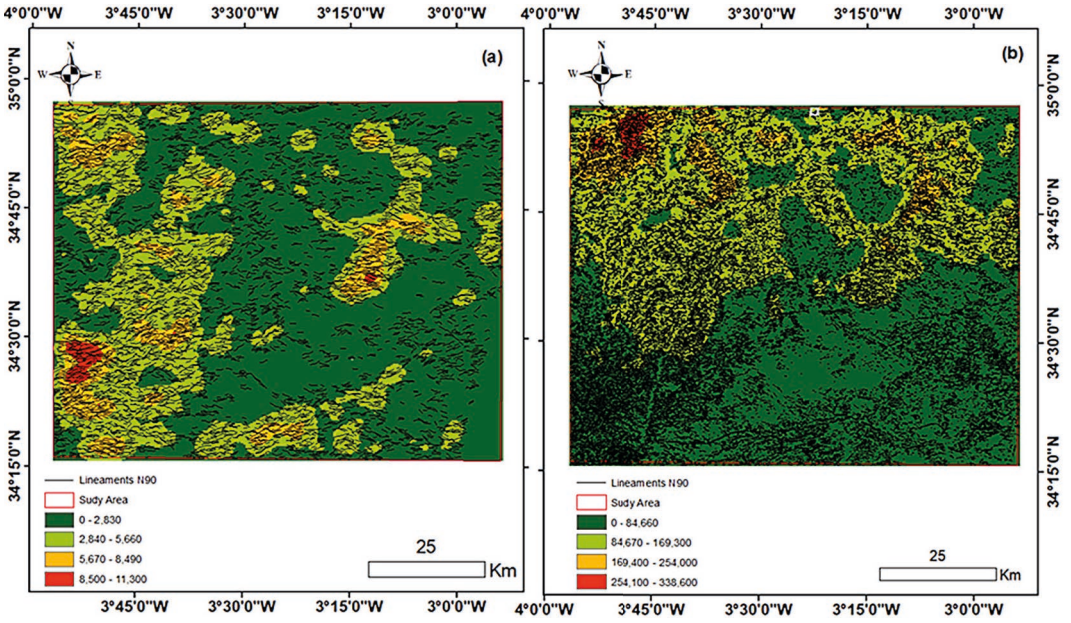

Figure 12. Lineament density for the N90 directional filters

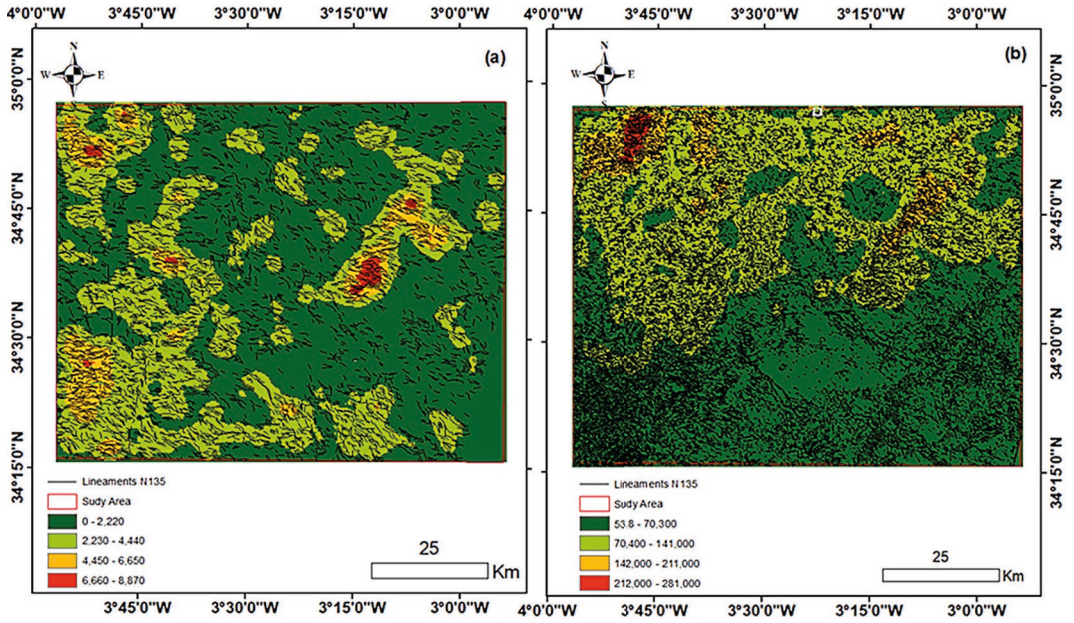

Figure 13. The lineament density for the directional filters N135 extracted from (a) Landsat-8 OLI and (b) Sentinel-2B

and more detailed maps for structural mapping (Javhar et al., 2019; Wang et al., 2018). Numerous studies have demonstrated the significant role of Landsat and Sentinel data, processed using remote sensing methods, in identifying geological lineaments. The results obtained in the study area reveal a notable variation in the orientations of lineament structures, including NE-SW, E-W, and NW-SE directions. These findings align with those of other researchers in similar geological contexts in Morocco and other countries. For instance, the studies conducted by Farah et al. (Abdelouhed et al., 2021; Redouane et al., 2022) and Redouane et al. (Abdelouhed et al., 2021; Redouane et al., 2022) confirm these results. Additionally, specific lineament orientations in northern Morocco were identified through magnetic method studies, as documented in the research by Amar et al. (2015).

The three primary directions of tectonic discontinuities (faults) as depicted on the geological map align with the distribution of volcanic rock outcrops, and this alignment is further validated through the rose diagram depicting the distribution of extracted lineaments from the high-spatial-resolution Sentinel-2B satellite image (Figure 14). This study underscored the close relationship between regional geodynamic activities, which have led to the development of three predominant fault directions, ranked in order of significance as: NE-SW, E-W, and NW-SE (Figure 15). These fault orientations have facilitated the emplacement of magmas and the formation of volcanic outcrops in these same three primary directions, as confirmed by the methodology employed in our research.

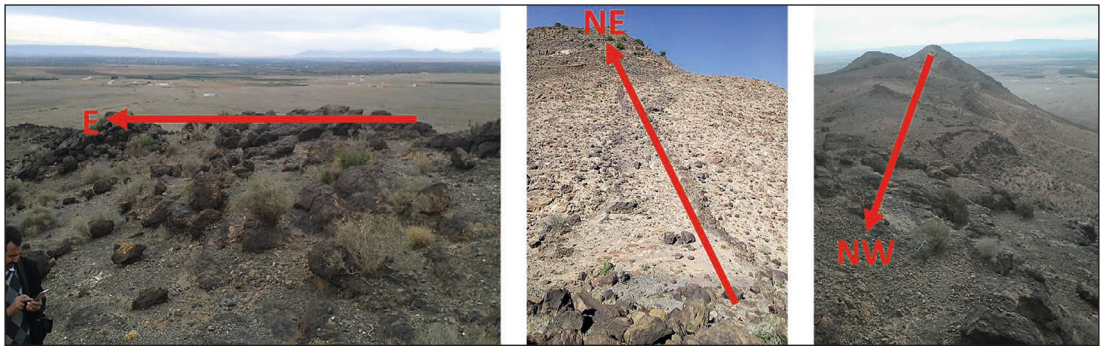

Figure 14. The primary directions of volcanic outcrop distribution in the study area

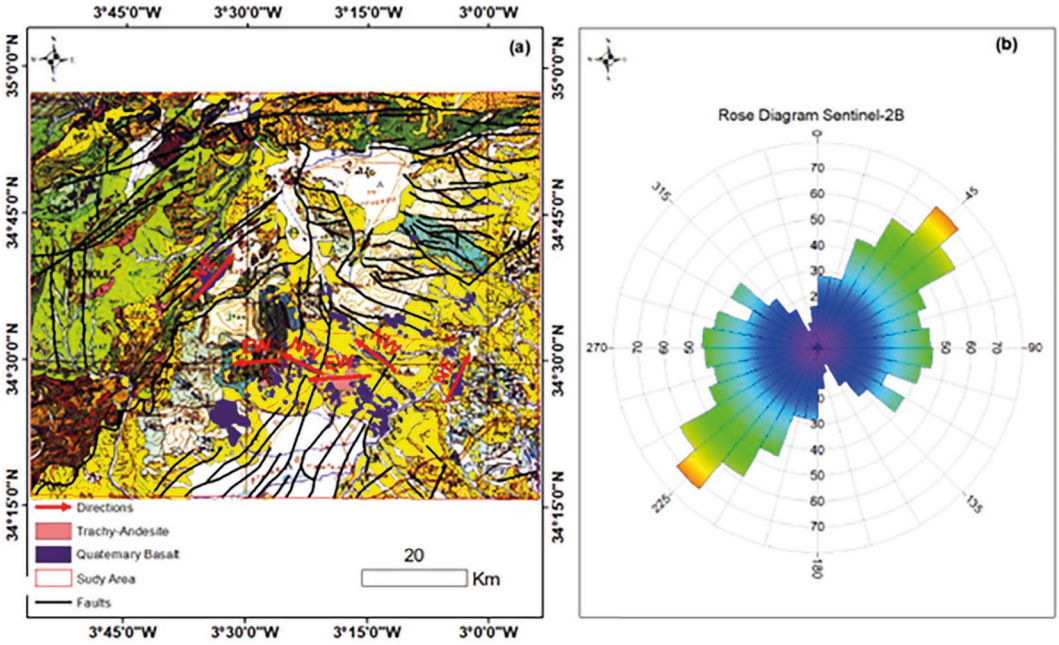

Figure 15. The three primary directions of volcanic outcrops (a) which align with faults in the study area, are confirmed by the rose diagram (b)

CONCLUSIONS

This study employed a lineament extraction approach utilizing remote sensing data. It combines automatic and manual extraction methods with geomatic tools to significantly reduce both the cost and time typically invested by geologists in creating a fracture map. This approach has enabled the production of a comprehensive lineament map for the Saka region and its vicinity. The methodology involves utilizing data sources to extract linear structures, followed by a thorough process of control and validation, resulting in detailed information regarding the area's fracturing. A comparison between the automatic extraction results and a manually generated map confirms the accuracy of this approach and its value in lineament identification.

Furthermore, density analysis was applied to investigate the connection between lineament concentration and the distribution of existing faults, while a geological map was utilized to better understand the correlation between density distribution and lithological units within the study area. The results obtained demonstrate a strong correlation between the directions of lineaments (mainly NE-SW, E-W, NW-SE) and faults, aligning with the distribution of volcanic outcrops in the Saka region and its surroundings.

Manual detection of geological lineaments is a more time-consuming process compared to automatic detection, yet it remains the method of choice for achieving a more reliable characterization of the detected lineaments.

Acknowledgements

The authors express their gratitude to the editor and the anonymous reviewers for their valuable comments and suggestions, which have significantly contributed to enhancing this work.

REFERENCES

1. Abdelouhed F., Ahmed A., Abdellah A., Mohammed I. 2021. Lineament mapping in the Ikniouen area (eastern anti-atlas, Morocco) using Landsat-8 Oli and SRTM data. Remote sensing applications: society and environment, 23, 100606.
2. Abdullah A., Nassr S., Ghaleeb A. 2013. Landsat ETM-7 for lineament mapping using automatic extraction technique in the SW part of Taiz Area, Yemen. Global Journal of Human-Social Science Research, 13, 34-38.
3. Adiri Z., El Harti A., Jellouli A., Lhissou R., Maacha L., Azmi M., Zouhair M., Bachaoui E.M. 2017. Comparison of Landsat-8, ASTER and Sentinel 1 satellite remote sensing data in automatic lineaments extraction: A case study of Sidi Flah-Bouskour inlier, Moroccan Anti Atlas. Advances in Space Research, 60, 2355-2367.
4. Ahmadi H., Pekkan E. 2021. Fault-based geological

lineaments extraction using remote sensing and GIS – a review. Geosciences, 11, 183.

5. Alshayef M.S., Mohammed A.M., Javed A., Albaroot M.A. 2017. Manual and automatic extraction of lineaments from multispectral image in part of Al-Rawdah, Shabwah, Yemen by using remote sensing and GIS technology. International Journal of New Technology and Research 3, 263346.
6. Amar N., Khattach D., Kaufmann O. 2015. Etude quantitative des linéaments magnétiques du Nord du Maroc.
7. Arian M., Nouri R. 2015. Lineament Tectonics and Mineralizatin in Tarom Area, North Iran. Open Journal of Geology 5, 115.
8. Begeman C., Helder D., Leigh L., Pinkert C. 2022. Relative Radiometric Correction of Pushbroom Satellites Using the Yaw Maneuver. Remote Sensing, 14, 2820.
9. Bernini M., Boccaletti M., Gelati R., Moratti G., Papani G., Mokhtari J.E. 1999. Tectonics and sedimentation in the Taza-Guercif Basin, Northern Morocco: Implications for the Neogene Evolution of the Rif-Middle Atlas Orogenic system. Journal of Petroleum Geology, 22, 115-128.
10. Bhuiyan C. 2015. Hydrological characterisation of geological lineaments: a case study from the Aravalli terrain, India. Hydrogeology Journal, 23, 673.
11. Burns K.L., Brown G.H. 1978. The human perception of geological lineaments and other discrete features in remote sensing imagery: Signal strengths, noise levels and quality. Remote Sensing of Environment, 7, 163-176.
12. Caumon G., Collon-Drouaillet P., Le Carlier de Veslud C., Viseur S., Sausse J. 2009. Surface-based 3D modeling of geological structures. Mathematical geosciences, 41, 927-945.
13. Chaabouni R., Bouaziz S., Peresson H., Wolfgang J. 2012. Lineament analysis of South Jenein Area (Southern Tunisia) using remote sensing data and geographic information system. The Egyptian Journal of Remote Sensing and Space Science, 15, 197-206.
14. Cooley T., Anderson G.P., Felde G.W., Hoke M.L., Ratkowski A.J., Chetwynd J.H., Gardner J.A., Adler-Golden S.M., Matthew M.W., Berk A. 2002. FLAASH, a MODTRAN4-based atmospheric correction algorithm, its application and validation, in: IEEE international geoscience and remote sensing symposium. IEEE, 1414-1418.
15. Corgne S., Magagi R., Yergeau M., Sylla D. 2010. An integrated approach to hydro-geological lineament mapping of a semi-arid region of West Africa using Radarsat-1 and GIS. Remote Sensing of Environment, 114, 1863-1875.
16. Das S., Pardeshi S.D., Kulkarni P.P., Doke A. 2018. Extraction of lineaments from different azimuth angles using geospatial techniques: a case study of Pravara basin, Maharashtra, India. Arabian Journal of Geosciences, 11, 1-13.
17. EL Kati I. 2017. Evolution géodynamique du bassin néogène de Guercif (Maroc): Télédetection, Tectonique et Magnétostratigraphie (Thesis). Ibn Tofail, Kenitra, Maroc.
18. El Kati I., Nakhcha C., El Bakhchouch O., Tabyaoui H. 2018. Application of Aster and Sentinel-2A Images for geological mapping in arid regions: The Safsafate Area in the Neogen Guercif basin, Northern Morocco. Int. J. Adv. Remote Sens. GIS, 7, 2782-2792.
19. Elaaraj A., Lhachmi A., Tabyaoui H., Alitane A., Varasano A., Hitouri S., El Yousfi Y., Mohajane M., Essahlaoui N., Gueddari H. 2022. Remote Sensing Data for Geological Mapping in the Saka Region in Northeast Morocco: An Integrated Approach. Sustainability, 14, 15349.
20. El-Sawy K., Ibrahim A.M., El-Bastawesy M.A., El-Saud W.A. 2016. Automated, manual lineaments extraction and geospatial analysis for Cairo-Suez district (Northeastern Cairo-Egypt), using remote sensing and GIS. International Journal of Innovative Science, Engineering & Technology, 3, 491-500.
21. Glasser N.F., Ghiglione M.C. 2009. Structural, tectonic and glaciological controls on the evolution of fjord landscapes. Geomorphology, 105, 291-302.
22. Hashim M., Ahmad S., Johari M.A.M., Pour A.B. 2013. Automatic lineament extraction in a heavily vegetated region using Landsat Enhanced Thematic Mapper (ETM+) imagery. Advances in Space Research, 51, 874-890.
23. Hein J.R., Mizell K., Koschinsky A., Conrad T.A. 2013. Deep-ocean mineral deposits as a source of critical metals for high-and green-technology applications: Comparison with land-based resources. Ore Geology Reviews, 51, 1-14.
24. Hung L.Q., Batelaan O., De Smedt F. 2005. Lineament extraction and analysis, comparison of LANDSAT ETM and ASTER imagery. Case study: Suoimuoi tropical karst catchment, Vietnam, in: Remote sensing for environmental monitoring, GIS applications, and geology V. SPIE, 182-193.
25. Huntington J.F., Raiche A.P. 1978. A multi-attribute method for comparing geological lineament interpretations. Remote Sensing of Environment, 7, 145-161.
26. Javhar A., Chen X., Bao A., Jamshed A., Yunus M., Jovid A., Latipa T. 2019. Comparison of multi-resolution optical Landsat-8, Sentinel-2 and radar Sentinel-1 data for automatic lineament extraction: A case study of Alichur area, SE Pamir. Remote Sensing, 11, 778.

27. Joshi A.K. 1989. Automatic detection of lineaments from Landsat data, in: 12th Canadian Symposium on Remote Sensing Geoscience and Remote Sensing Symposium,. IEEE, 85-88.
28. Koçal A. 2004. A methodology for detection and evaluation of lineaments from satellite imagery (Master's Thesis). Middle East Technical University.
29. Koike K., Nagano S., Ohmi M. 1995. Lineament analysis of satellite images using a Segment Tracing Algorithm (STA). Computers & Geosciences, 21, 1091-1104.
30. Lachaine G. 1999. Structures géologiques et linéaments, Beauce (Québec): apport de la télédétection. Université de Sherbrooke.
31. Lu Y., Liu L., Xu G. 2016. Constraints of deep crustal structures on large deposits in the Cloncurry district, Australia: Evidence from spatial analysis. Ore Geology Reviews, 79, 316-331.
32. Lund K., Tysdal R.G., Evans K.V., Kunk M.J., Pillers R.M. 2011. Structural controls and evolution of gold-, silver-, and REE-bearing copper-cobalt ore deposits, Blackbird district, east-central Idaho: Epigenetic origins. Economic Geology, 106, 585-618.
33. Maged M., Mazlan H. 2010. Lineament mapping using multispectral remote sensing satellite data. International Journal of Physical Sciences, 5, 1501-1507.
34. Manuel R., Brito M.D.G., Chichorro M., Rosa C. 2017. Remote sensing for mineral exploration in central Portugal. Minerals, 7, 184.
35. Martinez J.-M., Guyot J.-L., Filizola N., Sondag F. 2009. Increase in suspended sediment discharge of the Amazon River assessed by monitoring network and satellite data. Catena, 79, 257-264.
36. Masoud A., Koike K. 2017. Applicability of computer-aided comprehensive tool (LINDA: LINeament Detection and Analysis) and shaded digital elevation model for characterizing and interpreting morphotectonic features from lineaments. Computers & Geosciences, 106, 89-100.
37. Masoud A., Koike K. 2006. Tectonic architecture through Landsat-7 ETM+/SRTM DEM-derived lineaments and relationship to the hydrogeologic setting in Siwa region, NW Egypt. Journal of African Earth Sciences, 45, 467-477.
38. Masoud A.A., Koike K. 2011. Auto-detection and integration of tectonically significant lineaments from SRTM DEM and remotely-sensed geophysical data. ISPRS journal of Photogrammetry and Remote sensing, 66, 818-832.
39. Mavrantza O., Argialas D.P. 2003. Implementation and evaluation of spatial filtering and edge detection techniques for lineament mapping: case study-Alevrada, Central Greece, in: Remote Sensing for Environmental Monitoring, GIS Applications, and Geology II. SPIE, 417-428.
40. Moore G.K., Hastings D.A. 1986. Digital processing of Landsat tm images for lineament occurrence and spatial frequency in sedimentary rocks. Geological Survey, Sioux Falls, SD (USA).
41. Negredo A.M., Replumaz A., Villaseñor A., Guillot S. 2007. Modeling the evolution of continental subduction processes in the Pamir–Hindu Kush region. Earth and Planetary Science Letters 259, 212-225. https://doi.org/10.1016/j.epsl.2007.04.043
42. Nguimbous-Kouoh J.J., Minyem D., Ghogomu R.T., Simon Ngos I.I.I., Manguelle-Dicoum E. 2019. Watersheds Morphometry and Structural Interpretation of Lineaments Extracted from SRTM Data in the Mayo-Kani Division Far-Nord Region,(Cameroon). Journal of Geosciences, 7, 54-65.
43. Paiva R.C., Durand M.T., Hossain F. 2015. Spatiotemporal interpolation of discharge across a river network by using synthetic SWOT satellite data. Water Resources Research, 51, 430-449.
44. Pour A.B., Hashim M. 2014. Structural geology mapping using PALSAR data in the Bau gold mining district, Sarawak, Malaysia. Advances in Space Research, 54, 644-654.
45. Rahnama M., Gloaguen R. 2014. TecLines: A MATLAB-based toolbox for tectonic lineament analysis from satellite images and DEMs, part 1: Line segment detection and extraction. Remote Sensing, 6, 5938-5958.
46. Rajendran S., Nasir S. 2019. ASTER capability in mapping of mineral resources of arid region: A review on mapping of mineral resources of the Sultanate of Oman. Ore Geology Reviews, 108, 33-53.
47. Ramli M.F., Yusof N., Yusoff M.K., Juahir H., Shafri H.Z.M. 2010. Lineament mapping and its application in landslide hazard assessment: a review. Bulletin of Engineering Geology and the Environment, 69, 215-233. https://doi.org/10.1007/s10064-009-0255-5
48. Redouane M., Mhamdi H.S., Haissen F., Raji M., Sadki O. 2022. Lineaments Extraction and Analysis Using Landsat 8 (OLI/TIRS) in the Northeast of Morocco. Open Journal of Geology, 12, 333-357.
49. Sarp G. 2005. Lineament analysis from satellite images, north-west of Ankara (Master's Thesis). Middle East Technical University.
50. Singh P.P., Garg R.D. 2013. Automatic road extraction from high resolution satellite image using adaptive global thresholding and morphological operations. Journal of the Indian Society of Remote Sensing, 41, 631-640.
51. Soto-Pinto C., Arellano-Baeza A., Sánchez G. 2013. A new code for automatic detection and analysis of the lineament patterns for geophysical and geological purposes (ADALGEO). Computers & geosciences, 57, 93-103.

52. Suzen M.L., Toprak V. 1998. Filtering of satellite images in geological lineament analyses: an application to a fault zone in Central Turkey. International journal of remote sensing, 19, 1101-1114.
53. Takorabt M., Toubal A.C., Haddoum H., Zerrouk S. 2018. Determining the role of lineaments in underground hydrodynamics using Landsat 7 ETM+ data, case of the Chott El Gharbi Basin (western Algeria). Arabian Journal of Geosciences, 11, 1-19.
54. Tyan C.-Y., Wang P.P. 1993. Image processing-enhancement, filtering and edge detection using the fuzzy logic approach, in: [Proceedings 1993] Second IEEE International Conference on Fuzzy Systems. IEEE, 600-605.
55. Valero S., Chanussot J., Benediktsson J.A., Talbot H., Waske B. 2010. Advanced directional mathematical morphology for the detection of the road network in very high resolution remote sensing images. Pattern Recognition Letters, 31, 1120-1127.
56. Wang D., Wan B., Qiu P., Su Y., Guo Q., Wang R., Sun F., Wu X. 2018. Evaluating the performance of Sentinel-2, Landsat 8 and Pléiades-1 in mapping mangrove extent and species. Remote Sensing, 10, 1468.
57. Wang J. 1993. LINDA – a system for automated linear feature detection and analysis. Canadian Journal of Remote Sensing, 19, 009-021.
58. Wang J., Howarth P.J. 1990. Use of the hough transform in automated lineament. IEEE transactions on geoscience and remote sensing, 28, 561-567.
59. Zhang X., Pazner M., Duke N. 2007. Lithologic and mineral information extraction for gold exploration using ASTER data in the south Chocolate Mountains (California). ISPRS Journal of Photogrammetry and Remote Sensing, 62, 271-282.
60. Zlatopolsky A.A. 1992. Program LESSA (Lineament Extraction and Stripe Statistical Analysis) automated linear image features analysis – experimental results. Computers & Geosciences, 18, 1121-1126.